Single Live Cell Assays with Label-free Optical Biosensor for the Development of Diagnostic Methods

Igor Sallai[1, 2)]
1) Nanobiosensorics Laboratory, Institute of Technical Physics and Materials Science, Centre for Energy Research, HUN-REN, Budapest, Hungary
2) Department of Electronics Technology, Budapest University of Technology and Economics, Budapest, Hungary
sallai.igor@ek.hun-ren.hu

***Abstract*—The collection of single-cell level information has become essential in the development of drug molecules, diagnostics, and therapeutics, as cellular responses measured at the population level often lack the resolution necessary to fully understand the underlying biological phenomena—whether in response to drugs, mechanical stimuli, or activation signals. Label-free optical biosensors offer an excellent platform for investigating such processes. This study presents a label-free resonant waveguide grating (RWG) method, developed using a fluidic system that includes a rotating fluid layer covering a sensor array and integrated microfluidic channels. We analyzed adhesion phenomena at the small-population level and the cellular responses to mechanically induced shear stress generated by fluid rotation. Our findings demonstrate that optically measured wavelength shift kinetics can accurately predict both the mechanical detachment dynamics of cells and the characteristics of the rotational flow field. Additionally, cellular responses to enzymatic digestion were clearly detectable and manifested as a significant reduction in near-surface cell mass.**

Keywords—biosensing, single-cell, label-free, fluidic flow, cellular activation, adhesion

I. INTRODUCTION

Measuring living cells in conditions similar to their unaltered, native physiological environments is crucial for accurately understanding cellular functions and behaviors. The presence of labeling agents, such as fluorescently conjugated monoclonal antibodies or differential staining dyes, can significantly modify cellular responses, potentially leading to misinterpretation of experimental results [1], [2]. Therefore, it is essential to develop measurement conditions that closely mimic physiological contexts to analyze authentic cellular functions and responses to various stimuli [3]. Label-free biosensor methods provide effective solutions to achieve this goal, enabling direct monitoring of cellular functions without interfering with cell integrity.

Label-free optical biosensors typically measure biomolecular interactions within an optical sensing volume, where biomolecules induce alterations in optical density and refractive index [4]. These optical changes modulate the propagation characteristics of the probing light, enabling sensitive detection of cellular responses. Well-based label-free biosensor platforms facilitate high-throughput screening and real-time monitoring with high temporal and spatial resolution [5]. Commonly employed surface-sensitive optical biosensor techniques include resonant waveguide grating (RWG), surface plasmon resonance (SPR), localized surface plasmon resonance (LSPR), and grating-coupled interferometry (GCI) [6], [7], [8], [9], [10]. In RWG biosensor technology, the sensor surface consists of a nanolithographically fabricated grating embedded within a waveguiding layer placed onto a transparent glass substrate [11]. This waveguiding layer typically exhibits a high refractive index, which is essential for effective signal propagation [12]. During measurement, the waveguide is illuminated by a broadband light source, and resonance occurs at specific wavelengths, coupling light into the waveguiding layer and resulting in partial propagation followed by reflection. An integral component of the RWG system is the complementary metal-oxide semiconductor (CMOS) camera, designed to detect changes in the resonant wavelength [13]. Upon coupling the light into the waveguide, an evanescent electromagnetic field is generated, which exponentially decays into the adjacent liquid medium. This field penetrates approximately 150–200 nm from the solid-liquid interface, allowing highly sensitive detection of cellular interactions and biomolecular events.

To accurately model human physiological conditions—particularly regions adjacent to fluid flow—in combination with sensor technologies, the integration of microfluidic systems is essential [14]. Microfluidics plays a critical role in lab-on-a-chip, organ-on-a-chip technologies and the development of point-of-care clinical diagnostics. The most significant fluidic system within the human body is the cardiovascular system [15]. Different shear forces are present in various regions of the cardiovascular system, including veins, arteries, arterioles, and capillaries, eliciting distinct responses from endothelial cells, circulating leukocytes, altered self-structures, and tumor cells [16]. Investigating cellular responses to mechanical stimuli, particularly shear stress, using label-free biosensor technologies is therefore crucial and represents an actively studied area in biomedical research [14], [15]. To fully understand the effects of shear stress at the population, single-cell, or subcellular level, it is essential to characterize the adhesion properties of cells, including adhesion forces and energies [17]. In addition to endothelial cells, flowing leukocytes exhibit analyzable adhesion properties. Specifically, monocytes that differentiate into interstitially patrolling macrophages and subsequently extravasate from the vascular compartment possess critical adhesion characteristics [18]. These characteristics arise due to differences in adhesion molecule expression among leukocyte subpopulations, selectin-mediated rolling mechanisms, and the recruitment of specific adhesion molecules during extravasation [19]. Once leukocytes migrate into the interstitial fluid, they rapidly become activated by altered self-structures, antigens, or

immune complexes [20]. These mechanisms can be effectively modeled using label-free biosensor measurements [21]. Such biosensors can be functionalized with adhesion-promoting extracellular matrix components, including fibronectin, laminin, or PLL-g-PEG-RGD, which specifically engage cell membrane-bound adhesion receptors, such as integrins and cadherins [7], [13]. Additionally, sensor surfaces can be modified with activating agents, including antigen-specific immunoglobulins or immune complexes. The subsequent analysis of cellular adhesion properties enables the translation of these adhesion signals into functional measures of immune cell activation [20]. Ultimately, these techniques offer promising platforms for developing immunofunctional diagnostics based on cellular response analysis [21].

II. Materials and Methods

A. Biosensor approach

Epic Benchtop and high-resolution Epic RWG biosensors are utilized to analyze cellular adhesion kinetics and responses to mechanical stimuli, particularly shear stress (Fig. 1.). The sensors are illuminated from below by transmitted light in incremental steps of 100 pm every 20 ms. The classical sensor platforms feature multi-well formats with 96, 384, or 1536 wells per plate. Each well contained a 2000 µm × 2000 µm waveguiding Nb_2O_5 layer with an embedded grating structure. A CMOS camera detects the reflected resonant wavelength component. The Epic Benchtop biosensor provides a maximum spatial resolution of 83 µm and temporal resolution of 3 sec., whereas the high-resolution Epic sensor offers improved performance with a maximum spatial resolution of 25 µm and maximum temporal resolution of 12 sec.

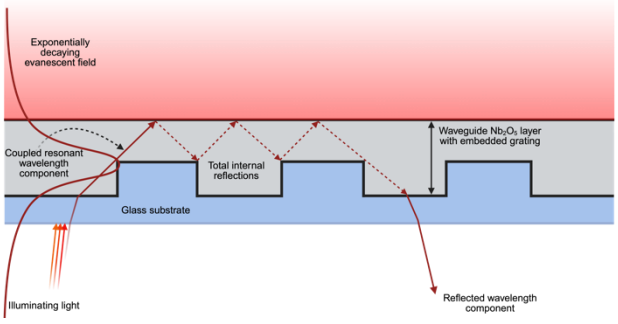

Fig. 1. The physical mechanism of resonant wavelength propagation within the Nb_2O_5 layer. (Created in BioRender. Sallai, I. (2025) https://BioRender.com/m417cho)

B. The custom-made well system

Two types of custom-made well plates were manufactured (Fig. 2.). In both cases, only the sensor plate was used, without standard commercial wells. One well design featured a diameter of 30000 µm and a height of 15000 µm. It encompassed 37 sensor surfaces, 8 of which were only partially located within the well. The second design had a diameter of 8800 µm and a height of 10650 µm. This well contained 6 sensor surfaces, with 4 only partially located within the well area. The distance between adjacent sensor surfaces was 2500 µm in all directions.

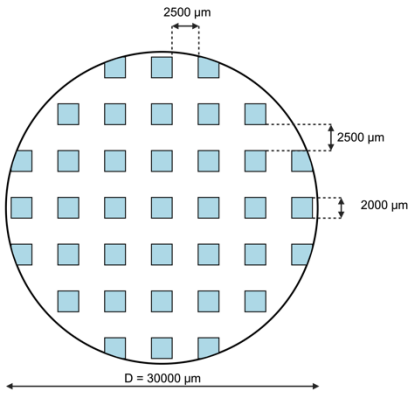

Fig. 2. Top-view layout and key dimensional parameters of the custom-made well used in the study including 37 sensor array. (Created in BioRender. Sallai, I. (2025) https://BioRender.com/m417cho)

C. Sensor surface functionalization

All wells containing sensor surfaces were functionalized to promote cellular adhesion. A 1 mg/mL solution of poly-L-lysine and polyethylene glycol graft copolymer (PLL-g-PEG) was mixed in a 1:1 ratio with a 1 mg/mL solution of RGD motif—containing poly-L-lysine and polyethylene glycol graft copolymer (PLL-g-PEG-RGD). In the case of the custom-made well containing 37 sensor surfaces, a final volume of 800 µL of the mixed solution was added to each well and incubated for 30 minutes (Fig. 3.). The polymers were dissolved in 10 mM HEPES-buffered Milli-Q water (pH 7.4), filtered through a 0.2 µm pore-size membrane, and stored at –20 °C until use.

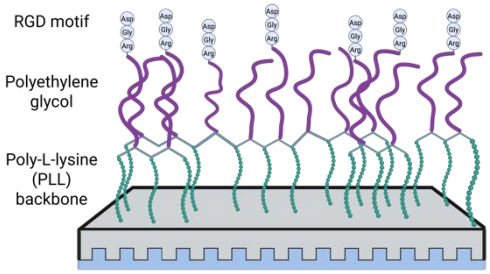

Fig. 3. Schematic representation of the functionalized sensor surface and polymer layer structure using a 1:1 mixture of PLL-g-PEG and PLL-g-PEG-RGD. (Created in BioRender. Sallai, I. (2025) https://BioRender.com/m417cho)

D. The used cell line preparation

The HeLa immortalized tumour cell line (ATCC: CCL-2, 93021013, Sigma-Aldrich) was utilised in the experimental procedures. The cells were cultivated in a humidified incubator maintained at a temperature of 37 °C, with the presence of 5% CO_2. The cells were maintained at an approximate density of 1–5 × 10^6 cells/mL, with the objective of creating a confluent monolayer. Cells were cultured in Dulbecco's Modified Eagle Medium (DMEM; pH 7.4), filtered through a 0.2 µm pore-size membrane. The medium was supplemented with 10% fetal bovine serum (FBS; Biowest SAS, France), 4 mM L-glutamine, 100 U/mL penicillin, and 100 µg/mL streptomycin to prevent contamination.

E. Measurements

After surface functionalization, a cell suspension prepared in 20 mM HEPES/HBSS buffer was added to the system, and cellular adhesion kinetics were monitored at the low population level for approximately 125 minutes. A low population level refers to the division of the sensor surface into pixel regions, where each pixel measures 83 × 83 µm. A single wavelength shift curve represents the collective response of the cells occupying that specific 83 × 83 µm area.

Subsequently, a magnetic stir bar (length: 20 mm, diameter: 6 mm) was introduced into the system. A rotating fan connected to a magnet generated an electromagnetic field, enabling the stir bar to levitate and rotate within the suspension. It was essential to minimize undesired mechanical vibrations during the experiment. During the rotation phase, different shear force conditions were established by rotating at 1800 RPM, 2400 RPM, and 2650 RPM. Cellular responses to each rotational condition were measured over a period of 1 hour. In one set of experiments, chemical detachment was also investigated by adding 100 µL of 10× trypsin-EDTA solution (final concentrations: 0.5% trypsin, 0.2% EDTA) to the suspension following the rotational phase. The solution was incubated over the adhered cells for 45 minutes.

F. Data evaluation, computational methods

Time-dependent adhesion kinetics data, generated by near-surface dynamic mass redistribution (DMR) events, were extracted using Aligner software (Corning, NY, USA). Kinetic data at the small population level were analyzed using a custom software tool developed in-house. Single-cell kinetic data acquired from high-resolution Epic measurements were also analyzed using a self-developed software package, which was implemented as a plugin in the Napari platform (https://napari.org/stable/). This user-friendly environment allows the adjustment of key parameters, such as the minimum neighborhood size—defining the minimal distance required for the software to identify individual cell adhesion or response signals. Another critical adjustable parameter is the minimum wavelength shift, which sets the threshold above which a signal is recognized as a valid cellular response. The software also supports baseline correction and background signal subtraction to improve data accuracy. Flow velocity and shear conditions were numerically (computational fluid dynamics — CFD) simulated using ANSYS CFX software.

III. Results

A. Epic Benchtop adhesion kinetics and rotational cell response analysis

The techniques and methodologies described by Kovács et al. will be critically reviewed and contextualized compared to other biosensor approaches and fluid handling methodologies. Fluid flow can elicit diverse responses from cell cultures, as clearly demonstrated in the study by Hoyle et al. (Fig. 4.) [22].

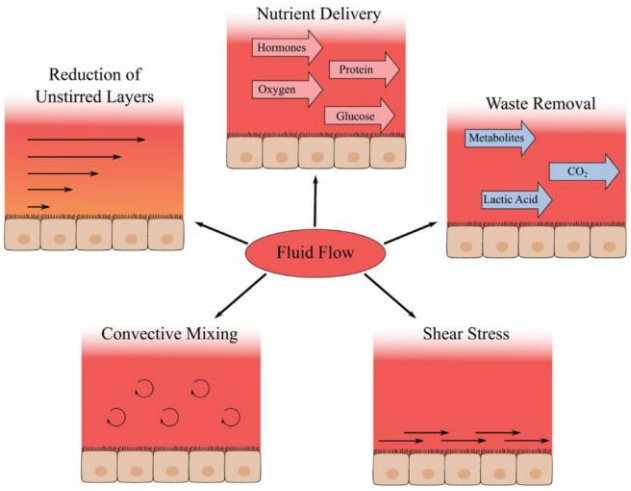

Fig. 4. The Fluid flow supports healthy cell growth through several mechanisms. It facilitates the continuous supply of fresh nutrients and the efficient removal of metabolic waste, thereby reducing nutritional stress on cells. The thinning of the unstirred layer and enhanced convective mixing further contribute to this process and are particularly advantageous in research applications such as transport studies. In addition, shear stress applied to the cell surface generates mechanical signals that elicit specific cellular responses. While such signals can help maintain physiological function, excessive or supraphysiological levels of shear stress may have detrimental effects on cells. Reproduced with permission from [22].

In the study by Kovács et al. (2021), a label-free resonant waveguide grating (RWG)-based optical biosensor array was integrated with a rotating fluidic setup to monitor whole-cell responses to varying fluid flow velocities on RGD-functionalized surfaces. This unique configuration enabled the simultaneous exposure of different sensor regions to distinct shear stress levels, allowing real-time, high-throughput kinetic measurements of cell adhesion and detachment at both small-population and population levels. The Epic Benchtop biosensor applied in the study offers a spatial resolution of 83 µm, which is sufficient to distinguish local, small-scale cell population responses. This resolution and temporal monitoring capability are comparable to those reported by Kumari et al. (2023) [23] and He et al. (2017) [24], while differing from the approaches of Hoyle et al. (2022) [22] and Young & Simmons (2010) [25], which focused primarily on broader, population-level analyses. The setup by Kovács et al. thus bridges a methodological gap, providing a spatially resolved analysis of adherent cell behavior under mechanical stimulation—similar in flexibility to the platform described by Burger & Ducrée (2012) [26].

In the study, the wavelength shift curves were normalized to the maximum shift value observed during the adhesion phase. These curves typically exhibited sigmoidal characteristics with low variance (Fig. 6.). A higher normalized maximum wavelength shift during the cellular adhesion phase indicates that more cells adhered to the sensor surface. Stable adhesion is further evidenced by cell spreading and the formation of adhesion focal points. These structures arise from biomolecular interactions between RGD motifs and cellular adhesion molecules, such as integrins, which are recruited to the focal adhesion sites. This recruitment enhances the wavelength shift, reflecting the establishment of strong and stable cell—surface interactions. Fig. 6. (a—c) shows the effects of applying different rotation frequencies after the 125-minute cellular adhesion phase. In contrast, Fig. 6. (d—f) presents the kinetic results from the

reference wells, where no rotation was applied following the adhesion phase. The data clearly indicate that even a rotation frequency of 1800 RPM induced partial detachment of the surface-adhered HeLa cell population. Increasing the frequency to 2400 and 2650 RPM further elevated the detachment rate, as reflected in the decreasing trend of the relative wavelength shift. The detachment rate is the percentage of the wavelength shift signal in the cell adhesion phase that is reduced by rotation compared to the maximum of the wavelength shift signal. While Kovács et al. primarily assessed cell adhesion and detachment kinetics, which relate indirectly to cellular integrin interactions, methods by He et al. (2017) [24] and Misun et al. (2016) [27] focused explicitly on secreted biomolecules, providing direct metabolic or secretomic insights (Fig. 5.).

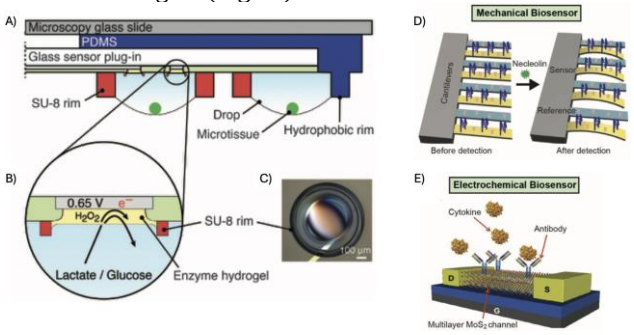

Fig. 5. A) Schematic cross-sectional representation of a biosensor integrated into a microfluidic hanging-drop system. In this setup, liquid droplets are suspended between SU-8 rim structures on a glass base and an overlying PDMS layer. The biosensors are positioned at the upper interface of the hanging droplets, enabling efficient interaction with the sample in a confined droplet environment. Reproduced with permission from [27]. B) Zoomed-in illustration showing the operational concept of an enzyme-functionalized biosensor. In this approach, enzymes such as glucose oxidase (GOx) or lactate oxidase (LOx) catalyze the conversion of glucose or lactate, generating hydrogen peroxide as a byproduct. This molecule is then detected electrochemically at a platinum electrode maintained at 0.65 V versus Ag/AgCl. Reproduced with permission from [27]. C) Photograph of a hydrogel-coated platinum electrode with integrated SU-8 guiding structures. The image highlights the SU-8 ring configuration, which allows for precise and reproducible deposition of hydrogel onto the sensing area of the electrode surface. Reproduced with permission from [27]. D) Conceptual drawing of a microcantilever biosensor targeting nucleolin. Sensing microcantilevers (shown in blue) are modified with nucleolin-specific aptamers and passivated with MCH, while control cantilevers (yellow) are only MCH-treated. Specific binding of nucleolin induces detectable mechanical deflection in the functionalized cantilevers. Reproduced with permission from [24]. E) Illustration of a multilayer molybdenum disulfide (MoS_2)-based field-effect transistor (FET) biosensor designed for TNF-α detection. This nanomaterial-based FET platform enables highly sensitive electrical readout of tumor necrosis factor-alpha binding events on the device surface. Reproduced with permission from [24].

This phenomenon can be attributed to complete cellular detachment as well as reduced adhesion strength as cells transition from a spread morphology to a more spherical shape. To confirm this observation, brightfield or phase-contrast microscopy should be conducted in parallel. Notably, not all cells detached completely, as the signal did not return to the cellular baseline. Higher rotation frequencies resulted in greater signal reductions; however, the difference in signal decline between 2400 and 2650 RPM was not pronounced.

Single-pixel kinetic analysis revealed that, at 1800 and 2400 RPM, signals dropped sharply with a high negative slope, followed by a transient phase lasting approximately 5—10 minutes, during which the signal slightly increased. This corresponds to the minimal normalized wavelength shift difference observed between the end of adhesion and the values recorded five minutes after the onset of rotation. Following this transient phase, the signal resumed a decreasing trend.

Interestingly, at 2650 RPM, some signals initially increased during the first five minutes. This may be explained by detached cells relocating randomly to other sensor regions or the cells more pressed against the sensor. To support this hypothesis, single-cell-level signal tracking and additional analysis is required to clarify the biological impact of high shear stress on cellular behavior.

Signals from the reference wells also exhibited a slight downward trend, which may be attributed to temperature fluctuations or their viability is reduced and they start to come up from the sensor surface.. Furthermore, attention must be given to the spatial saturation of the sensor surface. Overcrowding may act as a steric barrier, reducing the adhesion potential of cells. Therefore, it is essential to optimize the initial culturing density and normalize rotational signal data accordingly.

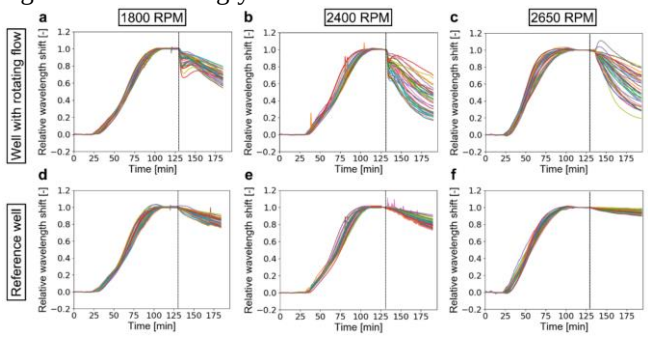

Fig. 6. Observed adhesion and rotation-induced wavelength shift signals for each pixel across all sensors (a—c), and the corresponding reference well signals during the adhesion and post-adhesion resting phases (d—f). Each wavelength shift curves connected to 83 × 83 µm sensor surface regions. All signals were normalized to the maximum wavelength shift value observed during the adhesion phase. The line indicates the time point at which rotation was initiated.

Fluid velocities in Kovács et al. ranged from near zero to ~1.16 m/s, controllable via rotation speed adjustments (1800-2650 RPM). This broad range and easy variability offer clear advantages compared to fixed-flow microchannel setups used by Shemesh et al. (2015) [28] or Shahbazi et al. (2021) [29].

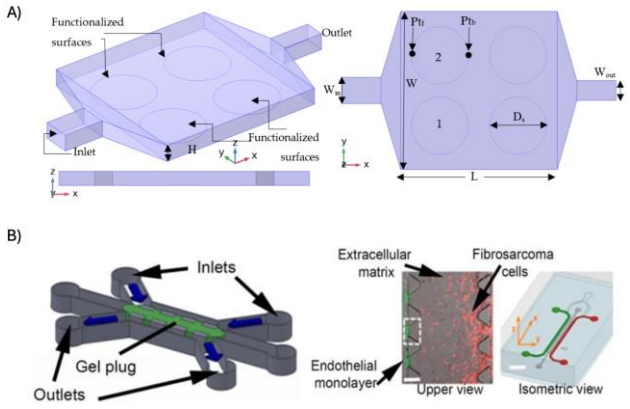

Fig. 7. A) Schematic representation of the microchamber layout used across four experimental configurations, including the original setup applied in the study. Reproduced with permission from [29]. B) Three-dimensional microfluidic platform engineered to regulate key microenvironmental

parameters—such as cell—cell communication and ECM-mimicking spatial organization—while enabling live-cell imaging. This system facilitates the investigation of tumor cell intravasation and endothelial barrier dynamics in the presence of cytokine-mediated endothelial activation and associated paracrine signaling interactions. Reproduced with permission from [28].

B. Results of numerical simulation

Another critical factor influencing the observed signals is the spatial location of the sensor pixel and its radial distance from the rotation axis. This necessitates numerical simulation of fluidic flow conditions for accurate interpretation. Computational fluid dynamics (CFD) simulations were performed for each applied rotation frequency. The results indicate that the fluid velocity at the center of the well is close to zero, and increases progressively with radial distance from the center. This increase continues up to a specific radial distance —which is approximately 9000 µm—, beyond which the velocity begins to decrease steadily toward the well wall corresponding to the numerical simulation (Fig. 8. a—c).

As a result, annular regions (i.e., zones at equal radial distances from the center) exhibit approximately uniform flow velocities. This geometrical feature allows for the comparison of kinetic data from different sensors located at the same radial distance, under similar hydrodynamic conditions (Fig. 8. d—f). The heatmap generated from the computed velocity distribution within the well closely corresponds to the average relative wavelength shift signals recorded from each sensor, which are connected to cellular response. This correlation underscores the relevance of the optical signal—i.e., the wavelength shift—as a predictor of local flow velocity. At a rotation frequency of 2400 RPM, the heatmap based on CFD velocity simulations and the averaged relative wavelength shift data display highly similar spatial patterns, confirming that shear-induced cellular responses can serve as indirect indicators of fluid flow conditions.

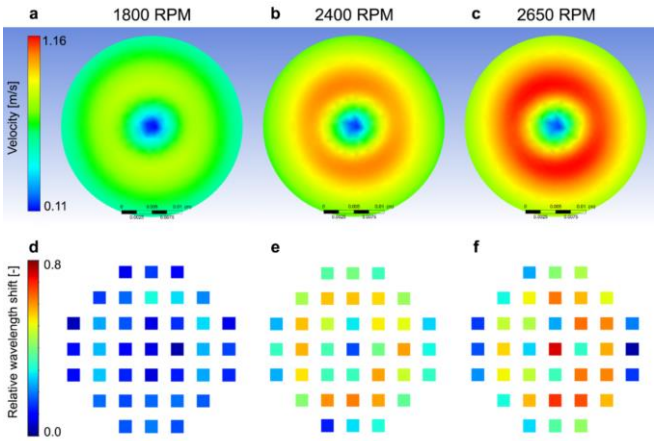

Fig. 8. Heatmaps of the CFD-simulated fluid flow velocity profiles from the top view of the well (a—c), and corresponding heatmaps of the average relative wavelength shift signals at the population level of living HeLa cells (d—f) [7]. Reproduced with permission from [7].

C. The effect of the simultaneously applied rotational shear stress and enzymatic treatment

In this experimental setup, measurements were conducted exclusively at a rotation frequency of 2400 RPM. Following the rotational phase, a 100 µL volume of 10× trypsin-EDTA solution (0.5% trypsin, 0.2% EDTA) was injected into the well via a connected microfluidic channel using a hydraulic pump and syringe.

.

The enzymatic treatment rapidly induced the detachment of a large proportion of the adhered cells, as evidenced by a steeper decline in the wavelength shift signals compared to the preceding rotational phase alone. To assess the combined effect of shear and enzymatic treatment, the signal changes have been analyzed at three different radial distances. The average relative wavelength shift—used as an indicator of detachment efficiency—was 0.33, 0.44, and 0.64, respectively, before enzymatic treatment. These values correlated with the computed flow velocities of 0.69, 0.73, and 0.96 m/s at the respective positions (Fig. 6.).

Based on these findings, it can be concluded that enzymatic treatment resulted in a 26% higher detachment rate compared to mechanical rotation alone. Such detailed, single-cell-level studies can be carried out in future experiments using the high-resolution Epic biosensor (Fig. 6.).

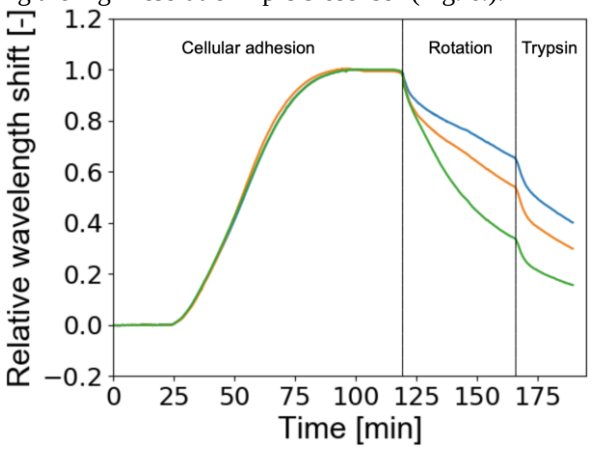

Fig. 9. Three different sensors, positioned at varying radial distances from the center of the well, were analyzed based on their average normalized wavelength shift kinetic signals [7]. The blue curve corresponds to a distance of 14230 µm, the orange curve to 13500 µm, and the green curve to 9000 µm from the center of the well. Following the cellular adhesion phase, a rotation frequency of 2400 RPM was applied for 45 minutes, after which trypsin-EDTA solution was introduced into the system. The computed fluid flow velocities at the respective sensor positions were 0.69, 0.73, and 0.96 m/s, while the corresponding normalized detachment rates were 0.33, 0.44, and 0.64. Reproduced with permission from [7].

Kovács et al. demonstrated high sensitivity, with critical fluid velocities precisely quantifiable (~0.5 m/s) and forces (around 910 nN) comparable to direct single-cell force measurements (Robotic FluidFM) [17], [30], [31]. This level of sensitivity is consistent with impedance-based sensors (Kim et al., 2021) and highly sensitive optical techniques (Kumari et al., 2023).

A distinct aspect of Kovács et al. is the use of rotational fluid flow, a novel approach compared to laminar flow systems in microchannels (Young & Simmons, 2010; Shemesh et al., 2015) [25], [28] and centrifugal systems (Burger & Ducrée, 2012) [26]. This rotational setup allowed varied simultaneous fluid velocities without the complexities of multiple pumps or channel architectures.

IV. DISCUSSION

Similar to all reviewed approaches, Kovács et al. successfully combined RWG biosensing with optical

microscopy, highlighting robust integration for direct visual validation of biosensor results.

It is advisable to complement these kinetic experiments with phase-contrast microscopy and cell count analysis to determine whether the observed signal decrease correlates linearly with cell number or follows a more complex relationship. Another important line of investigation is the assessment of cell viability, as some of the cells remaining on the surface after simultaneous rotation and enzymatic hydrolysis may be non-viable.

Numerical simulations of fluid flow velocities at various radial distances from the center of the well revealed that different rotation frequencies do not significantly alter the shape of the velocity profile. Instead, higher rotation frequencies increase the velocity magnitude at each radial position without modifying the overall profile (Fig. 10. A)). When fitting a curve to the velocity data as a function of radial distance, a fifth-order polynomial provides the best approximation. The maximum velocity points for each rotation frequency show a slight outward shift toward the well wall. The simulated velocity values range between 0 and 1.1 m/s. By analyzing sensors positioned at various radial locations, a greater number of data points (or "samples") can be obtained, improving statistical power. A strong correlation was observed between changes in the relative wavelength shift and both the radial distance and the shape of the velocity profile (Fig. 10. B)).

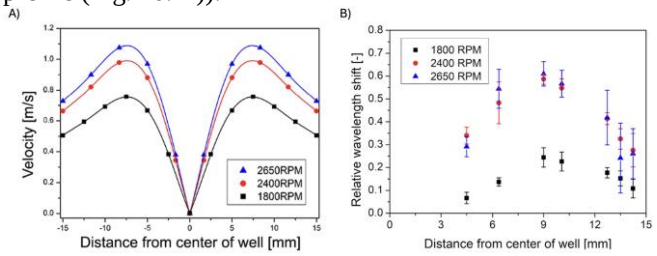

Fig. 10. Cross-sectional CFD-simulated fluid flow velocities as a function of radial distance from the well center (A), and corresponding relative wavelength shift values measured in sensor regions, also plotted as a function of radial distance (B) [7]. Reproduced with permission from [7].

These findings demonstrate that, in a rotating cylindrical system with known geometric and morphological parameters, it is possible to predict local fluid flow conditions based solely on the observed wavelength shift phenomenon. Furthermore, this approach enables population-level analysis of cellular responses to dynamically changing shear forces and chemical exposures.

V. Conclusion

In this study, we analyzed the effects of indirect fluid rotation—induced via magnetic coupling in a custom-made well plate—on live ovarian cancer HeLa cells. All experiments were conducted at the population level. The sigmoidal nature of cell adhesion was demonstrated by monitoring wavelength shift kinetics over time.

CFD simulations of the flow velocity profile within the well supported the analytical relevance of the average normalized wavelength shift. When plotted as a function of radial distance, the normalized wavelength shift values produced a curve closely matching the one derived from the simulated flow velocity data, indicating a strong correlation between the optical signal and local shear conditions.

Treatment with trypsin, an enzyme capable of disrupting bonds between adhesion molecules and the PLL-g-PEG/PLL-g-PEG-RGD—functionalized surface, enhanced cell detachment and significantly reduced the wavelength shift. This effect was primarily dependent on the radial position, consistent with the simulated flow velocity distribution.

High-throughput, simultaneous multi-condition assays, real-time kinetics, label-free sensing, and ease of tuning flow velocities clearly stand out as primary benefits. Compared to conventional microfluidic setups, this method uniquely provides a wide range of flow velocities on a single interface, significantly reducing experimental variability. The approach's complexity in setup calibration and ensuring stable rotational flow might be considered a drawback, although it remains less complex than multi-channel microfluidic systems. The potential noise introduced by mechanical rotation is also a factor, although minimal in this implementation. Kovács et al. achieved robust quantification of the critical flow velocity for cell detachment, simultaneously assessing mechanical and chemical stimuli impacts on cell populations. This combined stimulus capability, particularly without disturbing ongoing fluid flow, is a significant innovation.

We aim to analyze cellular responses to specific drug molecules during preclinical and developmental phases, as well as the adhesion and rotational wavelength shift kinetics following enzymatic hydrolysis of the glycocalyx layer surrounding the cells—thereby better modeling certain pathological conditions.

To achieve this, we plan to conduct our measurements using the setup illustrated in Fig. 2., panel B. In addition, we intend to investigate further cell lines and complex primary cell cultures—such as brain endothelial cells and human peripheral blood leukocytes—under the same experimental concept, to uncover the biological mechanisms underlying the observed flow-induced cellular responses and their potential diagnostic relevance.

Acknowledgment

The research was supported by the National Research, Development and Innovation Office PD 134195 (for Sz. Z.), the National Research, Development and Innovation Fund TKP2021-EGA-04, and the HUN-REN Hungarian Research Network.

References

[1] Brian T. Cunningham, B. T. Cunningham, Lance G. Laing, and L. G. Laing, "Advantages and application of label-free detection assays in drug screening.," *Expert Opin. Drug Discov.*, vol. 3, no. 8, pp. 891–901, Jul. 2008, doi: 10.1517/17460441.3.8.891.

[2] U. Schnell, F. Dijk, K. A. Sjollema, and B. N. G. Giepmans, "Immunolabeling artifacts and the need for live-cell imaging," *Nat. Methods*, vol. 9, no. 2, pp. 152–158, Feb. 2012, doi: 10.1038/nmeth.1855.

[3] Jeremy J. Ramsden, J. J. Ramsden, Róbert Horváth, and R. Horvath, "Optical biosensors for cell adhesion," *J. Recept. Signal Transduct.*, vol. 29, pp. 211–223, Jul. 2009, doi: 10.1080/10799890903064119.

[4] Tzong-Hsien Lee, T.-H. Lee, Daniel Hirst, D. J. Hirst, Mibel [M-I] Isabel Aguilar, and M. Aguilar, "New insights into the molecular mechanisms of biomembrane structural changes and interactions by optical biosensor technology.," *Biochim. Biophys. Acta*, vol. 1848, no. 9, pp. 1868–1885, Sep. 2015, doi: 10.1016/j.bbamem.2015.05.012.

[5] A. M. Ferrie, O. D. Deichmann, Q. Wu, and Y. Fang, “High resolution resonant waveguide grating imager for cell cluster analysis under physiological condition,” *Appl. Phys. Lett.*, vol. 100, no. 22, p. 223701, May 2012, doi: 10.1063/1.4723691.

[6] Eniko Farkas *et al.*, “Kinetic monitoring of molecular interactions during surfactant-driven self-propelled droplet motion by high spatial resolution waveguide sensing.,” *J. Colloid Interface Sci.*, 2024, doi: 10.1016/j.jcis.2024.07.236.

[7] Kinga Dóra Kovács *et al.*, “Label-free tracking of whole-cell response on RGD functionalized surfaces to varied flow velocities generated by fluidic rotation.,” *J. Colloid Interface Sci.*, vol. 599, pp. 620–630, Apr. 2021, doi: 10.1016/j.jcis.2021.04.091.

[8] Yuhki Yanase *et al.*, “Detection of refractive index changes in individual living cells by means of surface plasmon resonance imaging.,” *Biosens. Bioelectron.*, vol. 26, no. 2, pp. 674–681, Oct. 2010, doi: 10.1016/j.bios.2010.06.065.

[9] A. Bonyár and Attila Bonyár, “Maximizing the Surface Sensitivity of LSPR Biosensors through Plasmon Coupling—Interparticle Gap Optimization for Dimers Using Computational Simulations,” *Biosensors*, vol. 11, no. 12, pp. 527–527, Dec. 2021, doi: 10.3390/bios11120527.

[10] Hajnalka Jankovics *et al.*, “Grating-coupled interferometry reveals binding kinetics and affinities of Ni ions to genetically engineered protein layers.,” *Sci. Rep.*, vol. 10, no. 1, p. 22253, 2020, doi: 10.1038/s41598-020-79226-w.

[11] Y. Fang, A. M. Ferrie, N. H. Fontaine, J. C. Mauro, and J. Balakrishnan, “Master Proof Resonant Waveguide Grating Biosensor for Living Cell Sensing,” *Biophys. J.*, Jan. 2006, doi: 10.1529/biophysj.105.077818.

[12] András Saftics *et al.*, “Data evaluation for surface-sensitive label-free methods to obtain real-time kinetic and structural information of thin films: A practical review with related software packages,” *Adv. Colloid Interface Sci.*, vol. 294, p. 102431, Apr. 2021, doi: 10.1016/j.cis.2021.102431.

[13] N. Orgovan, B. Peter, S. Bősze, J. J. Ramsden, B. Szabó, and R. Horvath, “Dependence of cancer cell adhesion kinetics on integrin ligand surface density measured by a high-throughput label-free resonant waveguide grating biosensor,” *Sci. Rep.*, vol. 4, no. 1, pp. 4034–4034, May 2015, doi: 10.1038/srep04034.

[14] Dimitry A. Chistiakov, D. A. Chistiakov, Alexander N. Orekhov, A. N. Orekhov, Yuri V. Bobryshev, and Y. V. Bobryshev, “Effects of shear stress on endothelial cells: go with the flow.,” *Acta Physiol.*, vol. 219, no. 2, pp. 382–408, Feb. 2017, doi: 10.1111/apha.12725.

[15] Huaying Chen *et al.*, “Microfluidic models of physiological or pathological flow shear stress for cell biology, disease modeling and drug development,” *Trends Anal. Chem.*, vol. 117, pp. 186–199, Aug. 2019, doi: 10.1016/j.trac.2019.06.023.

[16] Michalina Janiszewska *et al.*, “Cell adhesion in cancer: Beyond the migration of single cells.,” *J. Biol. Chem.*, vol. 295, no. 8, pp. 2495–2505, Feb. 2020, doi: 10.1074/jbc.rev119.007759.

[17] Milán Sztilkovics *et al.*, “Single-cell adhesion force kinetics of cell populations from combined label-free optical biosensor and robotic fluidic force microscopy.,” *Sci. Rep.*, vol. 10, no. 1, pp. 61–61, Jan. 2020, doi: 10.1038/s41598-019-56898-7.

[18] Peter L. Hordijk and P. L. Hordijk, “Recent insights into endothelial control of leukocyte extravasation,” *Cell. Mol. Life Sci.*, vol. 73, no. 8, pp. 1591–1608, Jan. 2016, doi: 10.1007/s00018-016-2136-y.

[19] Melissa K. Callahan, M. K. Callahan, Richard M. Ransohoff, and R. M. Ransohoff, “Analysis of leukocyte extravasation across the blood-brain barrier: conceptual and technical aspects.,” *Curr. Allergy Asthma Rep.*, vol. 4, no. 1, pp. 65–73, Jan. 2004, doi: 10.1007/s11882-004-0046-9.

[20] L. L. Lu, T. J. Suscovich, T. J. Suscovich, S. M. Fortune, and G. Alter, “Beyond binding: antibody effector functions in infectious diseases.,” *Nat. Rev. Immunol.*, vol. 18, no. 1, pp. 46–61, Jan. 2018, doi: 10.1038/nri.2017.106.

[21] Zoltán Szittner *et al.*, “Functional blood cell analysis by label-free biosensors and single-cell technologies,” *Adv. Colloid Interface Sci.*, pp. 102727–102727, Jul. 2022, doi: 10.1016/j.cis.2022.102727.

[22] H. W. Hoyle, C. M. L. Stenger, and S. A. Przyborski, “Design considerations of benchtop fluid flow bioreactors for bio-engineered tissue equivalents in vitro,” *Biomater. Biosyst.*, vol. 8, p. 100063, Dec. 2022, doi: 10.1016/j.bbiosy.2022.100063.

[23] S. Kumari *et al.*, “Microfluidic Platforms for Single Cell Analysis: Applications in Cellular Manipulation and Optical Biosensing,” *Chemosensors*, vol. 11, no. 2, p. 107, Feb. 2023, doi: 10.3390/chemosensors11020107.

[24] J. He, A. T. Brimmo, M. A. Qasaimeh, P. Chen, and W. Chen, “Recent Advances and Perspectives in Microfluidics-Based Single-Cell Biosensing Techniques,” *Small Methods*, vol. 1, no. 10, p. 1700192, Oct. 2017, doi: 10.1002/smtd.201700192.

[25] E. W. K. Young and C. A. Simmons, “Macro- and microscale fluid flow systems for endothelial cell biology,” *Lab Chip*, vol. 10, no. 2, pp. 143–160, 2010, doi: 10.1039/B913390A.

[26] R. Burger and J. Ducrée, “Handling and analysis of cells and bioparticles on centrifugal microfluidic platforms,” *Expert Rev. Mol. Diagn.*, vol. 12, no. 4, pp. 407–421, May 2012, doi: 10.1586/erm.12.28.

[27] P. M. Misun, J. Rothe, Y. R. F. Schmid, A. Hierlemann, and O. Frey, “Multi-analyte biosensor interface for real-time monitoring of 3D microtissue spheroids in hanging-drop networks,” *Microsyst. Nanoeng.*, vol. 2, no. 1, p. 16022, Jun. 2016, doi: 10.1038/micronano.2016.22.

[28] J. Shemesh, I. Jalilian, A. Shi, G. Heng Yeoh, M. L. Knothe Tate, and M. Ebrahimi Warkiani, “Flow-induced stress on adherent cells in microfluidic devices,” *Lab. Chip*, vol. 15, no. 21, pp. 4114–4127, 2015, doi: 10.1039/C5LC00633C.

[29] F. Shahbazi, M. Souri, M. Jabbari, and A. Keshmiri, “Flow Control Techniques for Enhancing the Bio-Recognition Performance of Microfluidic-Integrated Biosensors,” *Appl. Sci.*, vol. 11, no. 15, p. 7168, Aug. 2021, doi: 10.3390/app11157168.

[30] Á. G. Nagy, N. Kanyó, A. Vörös, I. Székács, A. Bonyár, and R. Horvath, “Population distributions of single-cell adhesion parameters during the cell cycle from high-throughput robotic fluidic force microscopy,” *Sci. Rep.*, vol. 12, no. 1, p. 7747, May 2022, doi: 10.1038/s41598-022-11770-z.

[31] Á. G. Nagy, I. Székács, A. Bonyár, and R. Horvath, “Cell-substratum and cell-cell adhesion forces and single-cell mechanical properties in mono- and multilayer assemblies from robotic fluidic force microscopy,” *Eur. J. Cell Biol.*, vol. 101, no. 4, p. 151273, Sep. 2022, doi: 10.1016/j.ejcb.2022.151273.